37

Acoustic modelling of large aftertreatment devices with multimodal incident sound fields

F. D. Denia[♭],[1], E. M. Sánchez-Orgaz[♭], J. Martínez-Casas[♭], J. Carballeira[♭] and L. Baeza[♭]

(♭) Instituto de Ingeniería Mecánica y Biomecánica (I2MB),
Universitat Politècnica de València
Camino de Vera s/n, Valencia, Spain.

1 Introduction

Large silencers are commonly used to attenuate noise in many ventilation applications, gas turbine systems, as well as large internal combustions engines (trucks, freight trains, etc.), among others. For their acoustic modelling and design, the well-established computational methods considered for the relatively small automotive exhaust silencers [1-8] can be extended. As these models for small devices usually assume that plane waves are present in the inlet/oulet ducts (even if higher order acoustic modes are propagating inside the silencer), some problems may arise. If numerical methods such as the finite element method (FEM) are applied [2, 3], a large increase in the number of degrees of freedom is required to achieve sufficiently accurate predictions at higher frequencies. When analytical approaches [4-8] are taken into account, the increase in the number of propagating higher order modes for large configurations significantly affects the silencer performance [9]. This influence is associated not only with the modes inside the silencer, but also with the modes present in the incident sound field within the inlet port [10-13]. It is worth noting that, for large inlet ducts, the incident plane wave excitation hypothesis no longer holds, and multimodal excitation is necessary.

The previous comments can be extended to a number of aftertreatment devices (ATD) such catalytic converters and particulate filters. While their acoustic attenuation performance can be assessed accurately for sizes typical of small automotive exhaust systems [14-19], further research is required for large ATD since the ducts and chambers involved are big enough to allow higher order modes to propagate inside the device as well as along the inlet/outlet ports. Accordingly, in this article the mode matching method is applied to the compatibility conditions of the three-dimensional (3D) acoustic fields at the ATD geometric discontinuities, leading to the computation of the complex wave amplitudes in all the subdomains involved and the corresponding transmission loss (TL). To have a realistic model, 3D propagation must be considered in the inlet/outlet ducts and chambers, while 1D wave propagation has to be assumed along the small capillaries of the catalytic converter/particulate filter monoliths of the ATD; therefore, these monoliths can be replaced by plane wave four-pole transfer matrices from an acoustical point of view [17-19]. On the other hand, for large ATD inlet ducts such as those found in heavy-duty and off-road engines, the usual models with plane incident wave excitation are not accurate since the onset of higher order incident modes in the inlet duct is expected for the frequency range of interest. Therefore,

[1] fdenia@mcm.upv.es

a TL variation is likely to occur depending on these modes, similar to the results found in large dissipative silencers [9]. Results are presented for three different multimodal incident sound field hypotheses [20]: equal modal amplitude (EMA), equal modal power (EMP) and equal modal energy density (EMED). A relevant influence on the sound attenuation is found for the test problems considered in the current investigation.

2 Overview of the acoustic problem

Figure 1.1 shows a circular concentric ATD including a monolith. As shown in recent studies [19], the sound attenuation of an exhaust device incorporating a monolith can be properly predicted if the monolith is replaced by a plane wave four-pole matrix providing a relationship between the acoustic fields at both sides of the capillary region. Therefore, the presence of higher order modes in the cylindrical inlet/outlet regions is combined with one dimensional wave propagation within the capillary ducts of the central monolith.

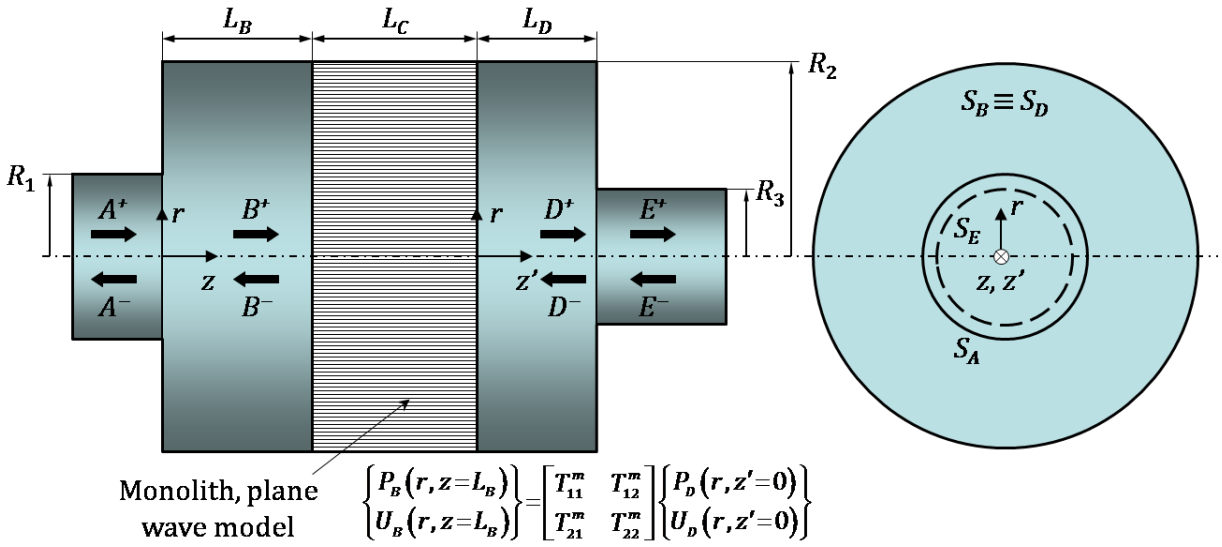

Figure 1: Scheme of a circular concentric ATD incorporating a monolith. The latter is replaced by a transfer matrix to model its acoustic behaviour.

In all the rigid ducts involved (A, B, D and E), the acoustic pressure and velocity fields can be written in terms of a series expansion. For example, the solution of the wave equation in region A is given by [4]

$$P_A(r,z) = \sum_{n=0}^{\infty} \left(A_n^+ e^{-jk_{A,n}z} + A_n^- e^{jk_{A,n}z} \right) \Psi_{A,n}(r) \tag{1}$$

$$U_A(r,z) = \frac{1}{\rho_0 \omega} \sum_{n=0}^{\infty} k_{A,n} \left(A_n^+ e^{-jk_{A,n}z} - A_n^- e^{jk_{A,n}z} \right) \Psi_{A,n}(r) \tag{2}$$

In the particular case of circular concentric ducts, the transversal pressure modes in Eqs. (1.1) and (1.2) are given by Bessel functions of the first kind and order zero, i.e. $\Psi_{A,n}(r) = J_0(\alpha_n r/R_1)$, where α_n are the roots satisfying the rigid wall boundary condition [4-7].
The complete acoustic field of the system requires the computation of the wave amplitudes $A_n^{\pm}$, $B_n^{\pm}$, $D_n^{\pm}$ and $E_n^{\pm}$ in all the ducts. The continuity conditions of the acoustic fields at the interfaces between ducts A and B (inlet expansion), as well as ducts D and E (outlet contraction) are

taken into account. The mode matching method [4-7] is here applied to the previous continuity conditions of the acoustic fields at all the interfaces to couple the solutions of the wave equation in the corresponding ATD subcomponents [19]. Regarding the capillary ducts, the acoustic coupling between both sides of the monolith (at the interfaces $S_B \equiv S_D$, see Figure 1.1) can be expressed as [14-19]

$$P_B(r, z = L_B) = T_{11}^m P_D(r, z' = 0) + T_{12}^m U_D(r, z' = 0) \text{ on } S_B \equiv S_D \tag{3}$$

$$U_B(r, z = L_B) = T_{21}^m P_D(r, z' = 0) + T_{22}^m U_D(r, z' = 0) \text{ on } S_B \equiv S_D \tag{4}$$

In matrix form yields

$$\begin{Bmatrix} P_B(r, z = L_B) \\ U_B(r, z = L_B) \end{Bmatrix} = \begin{bmatrix} T_{11}^m & T_{12}^m \\ T_{21}^m & T_{22}^m \end{bmatrix} \begin{Bmatrix} P_D(r, z' = 0) \\ U_D(r, z' = 0) \end{Bmatrix} \text{ on } S_B \equiv S_D \tag{5}$$

2.1 Mode matching method. Equations associated with the monolith

The equations and integrals associated with the inlet expansion and outlet contraction are omitted here for the sake of brevity. It is worth noting that advantage can be taken from the orthogonality properties of the rigid duct transversal modes, thus reducing the computational effort of the mode matching approach. Computational details of the corresponding integrals can be found in references [1, 4-7, 19]. Here, the application of the mode matching method focuses on the monolith. Thus, Eqs. (1.3) and (1.4) are multiplied by the transversal mode $\Psi_{B,s}(r) = \Psi_{D,s}(r) = J_0(\alpha_n r/R_2)$, with $s = 0, 1, 2, \ldots, N_m$ (a suitable series truncation is considered). Integrating over $S_B \equiv S_D$, yields the following equations for $s = 0, 1, 2, \ldots, N_m$

$$B_s^+ e^{-jk_{B,s}L_B} + B_s^- e^{jk_{B,s}L_B} = T_{11}^m \left(D_s^+ + D_s^-\right) + T_{12}^m \frac{k_{D,s}}{\rho_0 \omega} \left(D_s^+ - D_s^-\right) \tag{6}$$

$$\frac{k_{B,s}}{\rho_0 \omega} B_s^+ e^{-jk_{B,s}L_B} - B_s^- e^{jk_{B,s}L_B} = T_{21}^m \left(D_s^+ + D_s^-\right) + T_{22}^m \frac{k_{D,s}}{\rho_0 \omega} \left(D_s^+ - D_s^-\right) \tag{7}$$

As indicated in [19], it is worth noting here that very simple algebraic expressions have been obtained, where neither integrations nor modal summations appear, relating directly wave coefficients with equal modal number. These equations do not depend on the transversal cross section, provided that its geometry is axially uniform.

2.2 Multimodal excitation

As indicated previously, plane wave propagation in the inlet/outlet ducts of large ATD no longer holds. Thus, a procedure to account for multimodal excitation is described here. This can be summarized in five main steps. Step 1 is associated with the computation of the number of propagating modes in each duct for a given excitation frequency. For the inlet, this includes the plane wave mode (always present) and the non-planar excitation modes up to N, obtained through the condition

$$k_{A,n} = \sqrt{k_0^2 - (\alpha_n / R_1)^2} \geq 0 \text{ for } n = 0, 1, ..., N \tag{8}$$

Note that N can vary during an ATD acoustic computation, increasing as the excitation frequency exceeds the cut-on frequencies of the successive transverse higher order modes. Step 2 requires

the computation of the excitation wave amplitudes A_n^+ of the inlet duct [9, 20]. If only a plane wave (PW) is included in the analysis, this yields

$$A_0^+ = 1; A_n^+ = 0 \text{ for } n > 0 \tag{9}$$

Alternative mode mixtures include *equal modal amplitude* (EMA), *equal modal power* (EMP) and *equal modal energy density* (EMED), the corresponding expression being as follows [20]:

$$A_n^+ = 1 \text{ for } n \leq N \text{ (EMA)} \tag{10}$$

$$A_n^+ = \sqrt{\left(\delta_n^2/N\right)\left(1/\mathrm{Re}\left(k_{A,n}/k_0\right)\right)} \text{ for } n \leq N \text{ (EMP)} \tag{11}$$

$$A_n^+ = \sqrt{\delta_n^2 \Big/ \sum_j^N \mathrm{Re}\left(k_{A,j}/k_0\right)} \text{ for } n \leq N \text{ (EMED)} \tag{12}$$

where δ_n depends on the integration of the transversal modes over the cross section [20]. Once the excitation wave amplitudes A_n^+ are known, the mode matching system of equations is solved in step 3. While the treatment of the monolith has been outlined previously in Section 1.2.1, the reader is referred to reference [19] for details of the complete mode matching equations. Then, step 4 implies the computation of the acoustic incident/transmitted power at the end sections of the inlet/outlet ducts:

$$Pot_{inc} = \int_S \frac{1}{2}\mathrm{Re}\left(P_{inc}U_{inc}^*\right)dS = \frac{\pi}{\rho_0\omega}\sum_{n=0}^{N} k_{A,n}|A_n^+|^2 \int_0^{R_1} J_0\left(\alpha_n r/R_1\right)^2 r dr \tag{13}$$

$$Pot_{trans} = \int_S \frac{1}{2}\mathrm{Re}\left(P_{trans}U_{trans}^*\right)dS = \frac{\pi}{\rho_0\omega}\sum_{n=0}^{N} k_{E,n}|E_n^+|^2 \int_0^{R_3} J_0\left(\alpha_n r/R_3\right)^2 r dr \tag{14}$$

And finally, in step 5 the transmission loss is evaluated as

$$TL(dB) = 10\log\left(\frac{Pot_{inc}}{Pot_{trans}}\right) \tag{15}$$

2.3 Acoustic modelling of the ATD monolith

Figure 1.2 shows examples of monoliths and schemes of the associated flow pattern. Catalytic converter capillaries have upstream and downstream ends open, while particulate filters capillaries are characterized by channel ends alternatively plugged to force the flow through the porous walls [15].

Figure 2: Monolith and flow pattern: (a) Catalytic converter (CC); (b) Particulate filter (PF).

As indicated previously, the acoustic modelling assumes plane wave propagation in the capillaries, that can be computed through transfer matrices involved in Eqs. (1.3)-(1.7), relating the acoustic fields at both sides of the monolithic region. For further details of the models implemented in the current investigation to obtain these matrices, the reader is referred to works [14, 15, 20].

3 Results and discussion

Two axisymmetric configurations with a catalytic converter monolith are considered for validation and computation purposes. In the first case, geometry 1 has inlet and outlet ducts defined by the radii $R_1 = R_3 = 0.125$ m, while the chambers and monolith are characterized by the radius $R_2 = 0.25$ m and the lengths $L_B = L_D = 0.1475$ m and $L_C = 0.175$ m (see Figure 1.1 for details). In the second case, geometry 2 is defined by the dimensions $R_1 = R_3 = 0.25$ m, $R_2 = 0.5$ m, $L_B = L_D = 0.475$ m and $L_C = 0.75$ m. It is worth noting that in this latter case radii have been doubled and thus more higher order modes will propagate. Cold flow hypotheses with $T = 25°$C are retained through the computations, the properties for the air being $c_0 = 346.1$ m/s and $\rho_0 = 1.184$ kg/m^3. Regarding the monolith acoustic model, the following values are assumed: resistivity $R = 1500$ Pa $\cdot$ s/m^2, porosity $\phi = 0.88$, geometrical factor $\alpha_g = 1.14$, dynamic viscosity $\mu = 1.837 \cdot 10^{-5}$ Pa $\cdot$ s, thermal conductivity $\kappa = 0.0255$ W/(m $\cdot$ K) and specific heat $C_p = 1006.4$ J/(kg $\cdot$ K). The detailed model for the four-pole matrix computation can be found in the bibliography [14, 20].

3.1 Geometry 1: $N = 1$

For the conditions associated with this case, the incident modal field has a maximum of one higher order mode ($N = 1$), the cut-on frequency being 1688.6 Hz [1]. As it can be seen in Figure 1.3, the mode mixture rules modify the attenuation above this frequency value; in general, when incident energy propagates in higher order modes this seems to have a positive impact on the performance of the aftertreatment device. As observed by Kirby and Lawrie for large dissipative silencers [9], the three different multimode excitations considered for the incident acoustic field yield comparable results in general, although EMA predictions are lower than both EMED and EMP predictions.

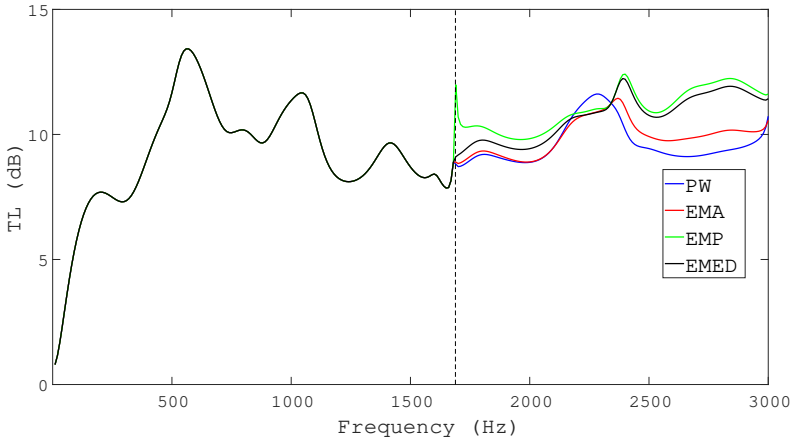

Figure 3: TL of an ATD (catalytic converter) for different modal excitations.

3.2 Geometry 2 (double radii): $N = 4$

In this case, the incident acoustic field has a maximum of four higher order modes ($N = 4$), the cut-on frequencies being 844.3 Hz, 1545.8 Hz, 2241.6 Hz and 2935.7 Hz respectively [1]. As shown in Figure 1.4, the main trends observed in the previous figure are also found here, the same comments being applicable in general. Anyway, the TL discrepancies among the different models seem to have decreased slightly in the high frequency range.

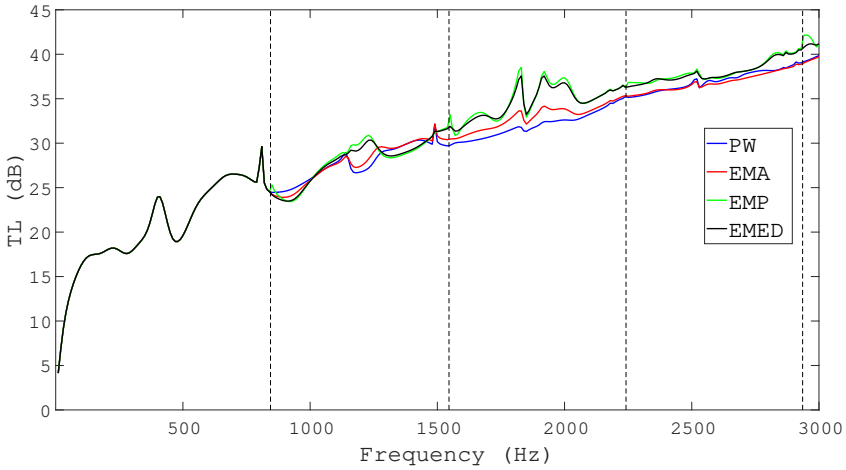

Figure 4: TL of an ATD (catalytic converter) for different modal excitations and double radii.

4 Conclusions

An accurate and efficient analytical method has been presented for the acoustic modelling of large ATD with a monolith. The model is based on the mode matching method and assumes 3D wave propagation in the inlet/outlet regions and 1D wave propagation in the monolith (these hypotheses have been validated experimentally in previous works). In large aftertreatment devices, plane wave (PW) propagation in the inlet/outlet ducts no longer holds for the frequency range of interest, and energy incident on the device propagating in higher order modes may have a strong impact on the acoustic attenuation performance. The specification of the incident modal field requires a knowledge of the source characteristics, but this is currently an open field of research and there is a lack of accurate representations as well as experimental validation. In addition to the PW model, several mode mixtures have been implemented: equal modal amplitude (EMA), equal modal power (EMP) and equal modal energy density (EMED). As expected, a strong influence of the mode mixture technique on the attenuation has been found. The three different multimode conditions adopted for the incident sound field can yield predictions that are consistent with the literature for some particular configurations, in the sense that at higher frequencies the acoustic performance of the exhaust device generally improves when energy from the source is carried by higher order modes (especially if dissipative effects are present in the analysis). However, the opposite trend has been also found for other geometries analysed in the current work (not shown for the sake of brevity). Thus, a plausible conclusion is that an accurate TL estimation in large aftertreatment devices requires the consideration of multimodal excitation, but the results are strongly dependent on the particular configuration under analysis and the mode mixture rule chosen. Literature seems to suggest that EMED is probably the most suitable model, although this depends on the noise source characteristics and further work is required.

5 Acknowledgements

The authors gratefully acknowledge Grants PID2020-112886RA-I00 and PID2020-118013RB-C21 funded by MCIN/AEI/10.13039/501100011033 and Project PROMETEO/2021/046 from Generalitat Valenciana.

References

[1] Munjal, M. L., Acoustics of Ducts and Mufflers. New York, Wiley, 2014.

[2] Antebas, A. G., Denia, F. D., Pedrosa, A. M., Fuenmayor, F. J., A finite element approach for the acoustic modeling of perforated dissipative mufflers with non-homogeneous properties. *Mathematical and Computer Modelling*, Volume(57):1970–1978, 2013.

[3] Denia, F. D., Sánchez-Orgaz, E. M., Martínez-Casas, J., Kirby, R., Finite element based acoustic analysis of dissipative silencers with high temperature and thermal-induced heterogeneity. *Finite Elements in Analysis and Design*, Volume(101):46–57, 2015.

[4] Selamet, A., Ji, J. L., Acoustic attenuation performance of circular expansion chambers with offset inlet/outlet: I. Analytical approach. *Journal of Sound and Vibration*, Volume(213):601–617, 1998.

[5] Kirby, R., Denia, F. D., Analytic mode matching for a circular dissipative silencer containing mean flow and a perforated pipe. *Journal of the Acoustical Society of America*, Volume(122):3471–3482, 2007.

[6] Denia, F. D., Selamet, A., Martínez, M. J., Fuenmayor, F. J., Sound attenuation of a circular multichamber hybrid muffler. *Noise Control Engineering Journal*, Volume(56):356–364, 2008.

[7] Denia, F. D., Antebas, A. G., Selamet, A., Pedrosa, A. M., Acoustic characteristics of circular dissipative reversing chamber mufflers. *Noise Control Engineering Journal*, Volume(59):234–246, 2011.

[8] Denia, F. D., Sánchez-Orgaz, E. M., Baeza, L., Kirby, R., Point collocation scheme in silencers with temperature gradient and mean flow. *Journal of Computational and Applied Mathematics*, Volume(291):127–141, 2016.

[9] Kirby, R., Lawrie, J. B., A point collocation approach to modelling large dissipative silencers. *Journal of Sound and Vibration*, Volume(286):313–339, 2005.

[10] Willimas, P. T., Kirby, R., The effect of higher order modes on the performance of large diameter dissipative silencers. Kraków, Forum Acusticum, 2014.

[11] Willimas, P. T., Åbom, M., Kirby, R., Hill, J., The influence of higher order incident modes on the performance of a hybrid reactive-dissipative splitter silencer. Boston, Acoustics'17, 2017.

[12] Kirby, R., Mimani, A., Attenuating sound in large ductwork using reactive and dissipative silencers. Ibiza, The 6^{th} Conference on Noise and Vibration Emerging Methods, 2018.

[13] Willimas, P. T., Kirby, R., Hill, J., Åbom, M., Malecki, C., Reducing low frequency tonal noise in large ducts using a hybrid reactive-dissipative silencer. *Applied Acoustics*, Volume(13):61–69, 2018.

[14] Selamet, A., Easwaran, J. M., Novak, J. M., Kach, R. A., Wave attenuation in catalytic converters: reactive versus dissipative effects. *Journal of the Acoustical Society of America*, Volume(13):935–943, 1998.

[15] Allam, S., Åbom, M., Sound propagation in an array of narrow porous channels with application to diesel particulate filters. *Journal of Sound and Vibration*, Volume(291):882–901, 2006.

[16] Denia, F. D., Antebas, A. G., Kirby, R., Fuenmayor, F. J., Multidimensional acoustic modelling of catalytic converters. Krákow, The Sixteenth International Congress on Sound and Vibration, 2009.

[17] Jiang, C., Wu, T. W., Xu, M. B., Cheng, C. Y. R., BEM modeling of mufflers with diesel particulate filters and catalytic converters. *Noise Control Engineering Journal*, Volume(58):243–250, 2010.

[18] Denia, F. D., Martínez-Casas, J., Baeza, L., Fuenmayor, F. J., Acoustic modelling of exhaust devices with nonconforming finite element meshes and transfer matrices. *Applied Acoustics*, Volume(73):713–722, 2012.

[19] Denia, F. D., Martínez-Casas, J., Carballeira, J., Nadal, E., Fuenmayor, F. J., Computational performance of analytical methods for the acoustic modelling of automotive exhaust devices incorporating monoliths. *Journal of Computational and Applied Mathematics*, Volume(330):995–1006, 2018.

[20] Mechel, F. P., Formulas of Acoustics. Berlin, Springer, 2008.